

# Efficiency and spectrum of internal $\gamma$ -ray burst shocks

D. Guetta<sup>1,2</sup>, M. Spada<sup>1,2</sup>, E. Waxman<sup>2</sup>

## ABSTRACT

We present an analysis of the Internal Shock Model of GRBs, where gamma-rays are produced by internal shocks within a relativistic wind. We show that observed GRB characteristics impose stringent constraints on wind and source parameters. We find that a significant fraction, of order 20%, of the wind kinetic energy can be converted to radiation, provided the distribution of Lorentz factors within the wind has a large variance and provided the minimum Lorentz factor is  $> \Gamma_{\pm} \approx 10^{2.5} L_{52}^{2/9}$ , where  $L = 10^{52} L_{52} \text{erg s}^{-1}$  is the wind luminosity. For a high,  $> 10\%$ , efficiency wind, spectral energy breaks in the 0.1 to 1 MeV range are obtained for sources with dynamical time  $R/c \lesssim 1 \text{ ms}$ , suggesting a possible explanation for the observed clustering of spectral break energies in this range. The lower limit  $\Gamma_{\pm}$  to wind Lorenz factor and the upper limit  $\approx 1(R/10^7 \text{cm})^{-5/6}$  MeV to observed break energies are set by Thomson optical depth due to  $e^{\pm}$  pairs produced by synchrotron photons. Natural consequences of the model are absence of bursts with peak emission energy significantly exceeding 1 MeV, and existence of low luminosity bursts with low, 1 keV to 10 keV, break energies.

*Subject headings:* gamma-rays: bursts - methods: numerical - radiation mechanisms: non-thermal

## 1. Introduction

The widely accepted interpretation of the phenomenology of  $\gamma$ -ray bursts (GRBs) is that the observable effects are due to the dissipation of the kinetic energy of a relativistically expanding wind, a “fireball” (see Mészáros 1995 and Piran 1996 for reviews). The discovery of GRB afterglow emission in X-ray (Costa et al. 1997), optical (van Paradijs et al. 1997) and radio wavelengths (Frail et al. 1997) confirmed (Waxman 1997, Wijers, Rees & Mészáros 1997), standard model predictions of afterglow (Paczynski & Rhoads 1993, Kats 1994, Mészáros & Rees 1997, Vietri 1997) that results from the collision of the expanding fireball with surrounding medium.

Both the spectrum and temporal dependence of afterglow emission are consistent with synchrotron emission of electrons accelerated to high energy at the shock wave driven by the

---

<sup>1</sup>Osservatorio di Arcetri L. E. Fermi 2 50100 Firenze, Italy

<sup>2</sup>Department of Condensed Matter Physics, Weizmann Institute, Rehovot 76100, Israel

fireball into its surrounding medium. The rapid temporal variability of  $\gamma$ -ray emission, i.e. of the GRB itself, imply, on the other hand, that the GRB is produced by internal shocks within the expanding wind (Woods & Loeb 1995, Sari & Piran 1997; Daigne & Mochkovitch, 1998; Panaitescu, Spada & Mészáros 1999). Both synchrotron and inverse-Compton emission from shock accelerated electrons have been proposed as the GRB emission mechanism. However, synchrotron emission is favored if the fireball is required to be “radiatively efficient,” i.e. if a significant fraction of the fireball energy is required to be converted to  $\gamma$ -rays (e.g. Derishev et al. 2000). Observations of GRB970508 afterglow implies a high radiative efficiency for this GRB (Frail Waxman & Kulkarni 2000), and X-ray afterglow observations imply that high radiative efficiency is required for most GRBs (Freedman & Waxman 2000).

Observations therefore suggest that the GRB emission is due to synchrotron emission of electrons accelerated by internal fireball shocks. This model faces, however, three major difficulties. First, it is generally argued that if  $\gamma$ -ray emission is due to internal shocks within the fireball, then only a small fraction,  $< 10^{-2}$ , of fireball energy is converted to  $\gamma$ -rays (Daigne & Mochkovitch, 1998; Kumar 1999, Kumar & Piran 1999, Spada, Panaitescu & Mészáros 2000). This is in conflict with the high radiative efficiency implied by afterglow observations. Second, the  $\gamma$ -ray emission of more than 60% of the GRBs observed by BATSE detectors is peaked at photon energies in the range of 50 keV to 300 keV (Brainerd et al. 1999). It is generally claimed that clustering of peak emission energy in this narrow energy range requires fine tuning of fireball model parameters, which should naturally produce a much wider range of peak emission energies. Finally, there is evidence that, at least in some cases, the GRB spectra at low energy is steeper than expected for synchrotron emission (Preece et al. 1998, Frontera et al. 2000).

The steep low energy spectra has led several authors to consider inverse-Compton emission as the source of  $\gamma$  radiation (e.g. Lazzati, et al 2000). However, steep low energy spectra may also be accounted for within the context of the synchrotron emission hypothesis by the effects of inverse-Compton suppression at low energies (Derishev et al. 2000) and by the contribution to observed  $\gamma$ -ray radiation of photospheric fireball emission (e.g. Mészáros & Rees 2000). As we show here (see discussion in §4), the contribution of latter effect is expected to be significant.

The main goal of the present paper is to determine the constraints imposed by GRB observations on the relativistic fireball wind parameters, and hence on the underlying source producing the wind, under the assumption that the observed radiation is due to synchrotron emission produced in internal wind shocks. In particular, we address the questions of whether, and under what conditions, high radiative efficiency can be obtained, and whether the clustering of peak emission energies can be naturally explained by the model.

It has been demonstrated in earlier work (e.g. Kobayashi et al. 1997; Beloborodov 2000), that high radiative efficiency may be obtained in the internal shock model provided the variance of the wind Lorentz factors distribution is large. Kobayashi et al. (1997) found  $\sim 10\%$  efficiency for uniform Lorentz factor distribution with maximum to minimum Lorentz factor ratio  $\approx 10$ ,

and Beloborodov (2000) demonstrated that the efficiency may approach 100% for non-uniform distributions with wide range of Lorentz factors<sup>3</sup>. In the analysis presented here we consider several issues which have not been addressed in earlier work: The constraints imposed on the model by the observed peak emission energy distribution, the effect of optical depth due to  $e^\pm$  pairs produced within the fireball wind, and the upper limit imposed on the maximum wind Lorentz factor by the acceleration process. The analysis presented here is also more general, as we study the dependence of radiative efficiency on a wider set of models parameters. We find that the radiative efficiency is limited to values well below the 80%–90% derived by Beloborodov. The inclusion of  $e^\pm$  pair optical depth effects is essential in determining both the efficiency and the peak emission energy.

High radiative efficiency clearly requires that a large fraction of the internal energy generated by internal shocks be carried by shock accelerated electrons, i.e. that the electron and proton energy densities be close to equipartition. Moreover, high radiative efficiency requires the magnetic field energy density to be not far below equipartition as well (e.g. Derishev et al. 2000). Thus, we assume in most our calculations that electrons, protons, and magnetic field energy densities are close to equipartition, and focus on the study of the dependence of observed  $\gamma$ -ray flux and spectrum on wind luminosity and on wind dynamical parameters (source size, variability time, Lorenz factor and mass distribution of shells within the wind). For completeness, we demonstrate using our calculations (in §3.2) that near equipartition is required in order for model predictions to be consistent with the observed peak emission energy distribution.

The model outline is presented in §2. The results of a numerical analysis of the model are presented and discussed in §3. The main conclusions are summarized in §4.

## 2. Outline of the model

In the fireball model of GRBs, a compact source, of linear scale  $R_0 \sim 10^6$  cm, produces a wind characterized by an average luminosity  $L_w \sim 10^{52} \text{ erg s}^{-1}$  and mass loss rate  $\dot{M} = L_w/\eta c^2$  ( $R_0 \sim 10^6$  cm corresponds to three times the Schwarzschild radius of a non-rotating, solar mass black hole, and  $L_w \sim 10^{52} \text{ erg s}^{-1}$  is the characteristic luminosity inferred from observations). At small radius, the wind bulk Lorentz factor,  $\Gamma$ , grows linearly with radius, until most of the wind energy is converted to kinetic energy and  $\Gamma$  saturates at  $\Gamma \sim \eta \sim 300$ .  $\eta \gtrsim 300$  is required to reduce the wind pair-production optical depth for observed high energy,  $> 100$  MeV, photons to less than unity. If  $\eta > \eta_* \approx (\sigma_T L_w / 4\pi m_p c^3 R_0)^{1/4} = 2 \times 10^3 (L_{w,52}/R_{0,6})^{1/4}$ , where  $L_w = 10^{52} L_{w,52} \text{ erg s}^{-1}$  and  $R_0 = 10^6 R_{0,6}$  cm, the wind becomes optically thin at  $\Gamma \approx \eta_* < \eta$ , and hence acceleration saturates at  $\Gamma \approx \eta_*$  and the remaining wind internal energy escapes as thermal radiation at

---

<sup>3</sup>Kobayashi & Sari (2001) similarly find  $\sim 60\%$  efficiency for non-uniform distribution of Lorentz factors over the range 10 to  $10^4$ .

$\sim 1$  MeV temperature. Variability of the source on time scale  $t_v$ , resulting in fluctuations in the wind bulk Lorentz factor  $\Gamma$  on similar time scale, then leads to internal shocks in the expanding fireball at a radius

$$R_i \approx \Gamma^2 c t_v = 3 \times 10^{11} \Gamma_2^2 t_{v,-3} \text{ cm}, \quad (1)$$

where  $\Gamma = 10^x \Gamma_x$ ,  $t_v = 10^{-3} t_{v,-3}$  s. If the Lorentz factor variability within the wind is significant, internal shocks reconvert a substantial part of the kinetic energy to internal energy. It is assumed that this energy is then radiated as  $\gamma$ -rays by synchrotron (and inverse-Compton) emission of shock-accelerated electrons.

In this work, we use an approximate model of the unsteady wind described in the preceding paragraph [following Kobayashi et al. 1997; Panaitescu, Spada, & Mészáros 1999; Spada, Panaitescu & Mészáros 2000 (SPM00)]. The wind evolution is followed starting at radii larger than the saturation radius, i.e. after the shells have already reached their final Lorenz factor following the acceleration phase, and the GRB photon flux and spectrum resulting from a series of internal shocks that occur within the wind at larger radii are calculated. We consider both synchrotron and the inverse-Compton emission, and take into account the effect of  $e^\pm$  pair production.

We approximate the wind flow as a set of discrete shells. Each shell is characterized by four parameters: ejection time  $t_j$ , where the subscript  $j$  denotes the  $j$ -th shell, Lorentz factor  $\Gamma_j$ , mass  $M_j$ , and width  $\Delta_j$ . Since the wind duration,  $t_w \sim 10$  s, is much larger than the dynamical time of the source,  $t_d \sim R_0/c$ , variability of the wind on a wide range of time scales,  $t_d < t_v < t_w$ , is possible. For simplicity, we consider a case where the wind variability is characterized by a single time scale  $t_w > t_v > t_d$ , in addition to the dynamical time scale of the source  $t_d$  and to the wind duration  $t_w$ . Thus, we consider shells of initial thickness  $\Delta_j = ct_d = R_0$ , ejected from the source at an average rate  $t_v^{-1}$ . The shell thickness may increase with time, due to variations in the expansion Lorenz factor across the shell. The Lorenz factor distribution across the shell depends on the entropy distribution, which is determined by the details of the ejection from the source. We therefore consider two extreme cases: uniform Lorenz factor across the shell, in which case the shell thickness is time independent, and order unity variation of LF across the shell,  $\Delta\Gamma/\Gamma \sim 1$ , in which case the shell thickness is given by  $\Delta_j = \max(R_0, R/\Gamma_j^2)$ .

We assume that the Lorenz factor (LF) of a given shell is independent of those of preceding shells, and consider 4 different LF distributions: uniform, modulated, bimodal, and lognormal. In the uniform distribution case, the shells' LFs are randomly drawn from a uniform distribution over the range  $\Gamma_m$  to  $\Gamma_M$ , where  $\Gamma_m < \Gamma_M$  are time independent. In the modulated case,  $\Gamma_M$  varies as  $\sin^2(2\pi t_j/t_w)$ . In the bimodal case, the LFs are drawn from a bimodal distribution,  $\Gamma_j = \Gamma_m$  or  $\Gamma_j = \Gamma_M$  with equal probability. Finally in the lognormal case, shell LFs are drawn from a lognormal distribution with an average  $\langle \Gamma \rangle = 1000$  and  $\langle \Gamma^2 \rangle^{1/2}/\langle \Gamma \rangle = 4$ , truncated at  $\Gamma > \eta_*$ .

The time intervals  $t_{j+1} - t_j$  are drawn randomly from a uniform distribution with an average value of  $t_v$ . The shell masses  $M_j$  are chosen to be either independent of  $j$ , or inversely proportional to  $\Gamma_j$ . That is, we consider the two qualitatively different possibilities: equal shell mass and

equal shell energy. The total mass is determined by the constraint  $\sum_{j=1}^N M_j \Gamma_j c^2 = L_w t_w$ , where  $N = t_w/t_v$ .

Once shell parameters are determined, we calculate the radii where collisions occur and determine the emission from each collision. We assume that following each collision the two colliding shells merge and continue to expand as a single shell. Under this assumption, the internal energy carried by the merged shell following the collision is

$$E_{in} = (M_1 \Gamma_1 + M_2 \Gamma_2 - (M_1 + M_2) \Gamma) c^2, \quad (2)$$

where

$$\Gamma = \sqrt{\frac{M_1 \Gamma_1 + M_2 \Gamma_2}{M_1/\Gamma_1 + M_2/\Gamma_2}} \quad (3)$$

is the expansion LF of the merged shell and  $M_{1,2}$ ,  $\Gamma_{1,2}$  are the masses and the LFs of the colliding shells. The dynamical efficiency  $\epsilon_d$ , defined as the fraction of total kinetic energy converted to internal energy, increases with the ratio of the fast and slow shell LFs, and, for a given ratio, is maximized for equal masses. The first collisions, for which the differences in the shell LFs are largest, are the most efficient.

In each collision a forward (FS) and a reverse (RS) shock are formed, propagating into forward and backward shells respectively. The plasma parameters behind each shock are determined by the Taub adiabat, requiring continuous energy density and velocity across the contact discontinuity separating the two shells (Panaitescu & Mészáros 1999). Since the energy density in the downstream regions of both shocks is similar, we divide the internal energy between the reverse and forward shock according to the ratio  $E_f/E_r = \Delta_f/k\Delta_r$ , where  $\Delta_{r,f}$  are the shell thicknesses prior to the collision and  $k$  is a factor of the order of few that takes into account the compression ratios of the two colliding shells.

The energy released in each shock is distributed among electrons, magnetic field and protons with fractions  $\epsilon_e$ ,  $\epsilon_B$  and  $1 - (\epsilon_e + \epsilon_B)$  respectively. We assume that electrons are accelerated by the shocks to a power-law distribution,  $dn_e/d\gamma_e \propto \gamma_e^{-p}$  for particle Lorentz factors  $\gamma_{\min} < \gamma_e < \gamma_{\max}$ .  $\gamma_{\max}$  is the electron Lorenz factor at which the synchrotron cooling time equals the acceleration time, estimated as the electron Larmor radius divided by  $c$ , while  $\gamma_{\min}$  is determined by the requirement that the energy carried by electrons be equal to  $\epsilon_e E_{in}$ .

The GRB energy spectrum and flux is derived by summing the contributions of individual shell collisions. For each collision, synchrotron and inverse-Compton emission by the shock-accelerated electrons is calculated. In order to achieve high radiative efficiency, electrons must radiatively loose most of their energy on a time scale shorter than shock shell crossing time. Under this condition, the synchrotron spectrum may be approximated as

$$F_\nu \propto \begin{cases} \nu^{-1/2} & \nu < \nu_{sy} \\ \nu^{-p/2} & \nu_{sy} < \nu \end{cases}, \quad (4)$$

where  $\nu_{sy}$  is the characteristic synchrotron emission frequency of electrons with  $\gamma \simeq \gamma_{\min}$ . The inverse Compton spectrum has a similar shape but is shifted to higher energy as described in SPM00. In determining the inverse-Compton flux, we take into account the Klein-Nishina suppression of the inverse-Compton cross section.

The photons radiated can be scattered by the electrons within the shell. The Thomson optical depth  $\tau_T$  for such scattering is evaluated by taking into account the electrons that were accelerated but have cooled radiatively while the shock crossed the shell, and those within the yet un-shocked part of the shell. The optical depth to Thomson scattering may be increased significantly beyond the value derived taking into account cooled shell electrons, due to the production of  $e^\pm$  pairs. This contribution has not been taken into account in previous analysis of the internal shock model, since for a uniform distribution of Lorentz factors, and under the hypothesis of equipartition, the break energy,  $h\nu_{sy}$ , in the shell co-moving frame is well below the pair production threshold. However, since the photon spectrum extends to high energy as a power law with spectral index  $-p/2 \approx -1$ , there is an equal number of photons per logarithmic energy intervals, and there may exist a large number of photons beyond the pair production threshold. The pairs produced by these photons may contribute significantly to the Thomson optical depth.

In order to take the effect of pair production into account, we determine for each collision the photon energy  $\epsilon_{\text{pairs}}$  for which the pair production optical depth  $\tau_{\gamma\gamma}$  equals unity. All the photons that have energies higher than  $\max(m_e c^2, \epsilon_{\text{pairs}})$  (measured in the shell frame) are assumed to form pairs, leading to a suppression of the high energy photon tail. We assume that the energy of photons that undergo pair production is converted to sub-relativistic pairs, which are taken into account in determining the Thomson optical depth.

We assume that a fraction  $(1 - e^{-\tau_{r,f}})/\tau_{r,f}$ , where  $\tau_{r,f}$  are the optical depths of the RS and FS, of the photons produced by each shock escapes and reaches the observer (The RS flux is also absorbed by the forward shell, and is thus further reduced by a factor  $e^{-\tau_f}$ ). The energy of the absorbed photons, as well as the internal energy which has not been converted to radiation, are converted back to ordered kinetic energy by adiabatic losses during the shell expansion. During this process, we take into account the increase in shell thickness by assuming this thickness grows as the shell's (comoving frame) speed of sound.

Our assumption, that following a collision two shells merger into one shell which expands with a single (uniform) Lorenz factor, leads to an overestimate of the reduction due to collisions of shell Lorenz factor variance. Clearly, the expansion of the shocked shells due to the pressure produced by the shocks results in the leading edge of the two shells moving faster (in the observer frame) than the trailing edge. It is therefore clear that the variance in Lorenz factor distribution following the collision is larger than obtained under our assumption of a “complete” merger. This, in turn, implies that a more detailed calculation of the shell merger process, which may require dividing the merged shells into several distinct shells following the collision, will enhance the overall efficiency of kinetic to thermal energy conversion. The magnitude of such enhancement

depends on the density and Lorenz factor distributions within the shells prior to the collision, and is expected to be of order unity. We therefore do not consider this effect in the approximate analysis presented in this paper.

### 3. Results and discussion

In this section we determine the dependence of the wind radiative efficiency  $\epsilon_\gamma$ , defined as the fraction of wind energy converted to radiation, and peak emission energy  $\varepsilon_p$ , the photon energy at which the maximum of  $\nu f_\nu$  is obtained, on wind model parameters. As explained in the introduction, we adopt electron and magnetic field energy fractions close to equipartition and analyze the dependence of  $\epsilon_\gamma$  and  $\varepsilon_p$  on wind luminosity, variability time, source size, and on the distribution of wind Lorentz factors and shell masses. We use  $\epsilon_e = 0.45$ ,  $\epsilon_B = 0.1$ , and  $p = 2$  throughout the paper, except in the calculations presented in Fig. 4, where smaller  $\epsilon_e$  and  $\epsilon_B$  values are assumed in order to demonstrate that near equipartition is required by observations. We first discuss in §3.1 the various Lorenz factor distributions described in §2. We then present a detailed discussion of the bimodal case, which best reproduces observed GRB characteristics, in §3.2.

#### 3.1. Comparison of various Lorenz factor distributions

Fig. 1 shows the results of numerical simulations of the model described in the previous section. Each panel shows  $\epsilon_\gamma$  versus  $\varepsilon_p$  for one of the LF distributions described in §2. Different points within each panel correspond to different choices of  $\Gamma_m$ ,  $\Gamma_M$  and  $t_v$ . Results are shown for  $10 < \Gamma_m < \Gamma_M < 2500$  and  $10^{-4} \text{ s} < t_v < 1 \text{ s}$ . We have assumed equal mass shells,  $R_0 = 10^6 \text{ cm}$ ,  $L_w = 10^{51} \text{ erg s}^{-1}$  and source redshift  $z = 1$  for all calculations. Results are presented for the two extreme assumptions on shell width evolution with radius described in §2, i.e. for both constant width  $\Delta = R_0$  and maximal expansion,  $\Delta = \max(R_0, R/\Gamma^2)$ .

Based on Fig. 1, a uniform LF distribution can be ruled out since the radiative efficiency is small,  $\epsilon_\gamma < 5\%$ . The low radiative efficiency in this case is due to low dynamical efficiency, i.e. to the fact that only a small fraction of the kinetic energy is converted to internal energy in collisions. In order to increase the dynamical efficiency it is necessary to either enhance the variance of the LF distribution of colliding shells at the first set of collisions (as is the case for bimodal or lognormal distributions) or to keep the variance moderate over a wind range of collision radii (as is the case for the modulated case).

In the modulated case the maximum dynamical efficiency is 40%. The first collisions remove the initial random differences and the merged shells have LFs near the ejection average value  $\langle \Gamma \rangle = (\Gamma_m + \Gamma_M)/2$ . If the wind is homogeneous  $\langle \Gamma \rangle$  is similar for all shells, resulting in a steady decrease of  $\epsilon_d$  during the wind expansion. If the range of LFs is varying on time scale of order

of  $t_w$ ,  $\langle \Gamma \rangle$  reflects the initial modulation of  $\Gamma_M$  and larger radii collisions that are dynamically efficient are still possible. Thus, a modulation in the wind can solve the efficiency problem ( $\epsilon_\gamma \approx 10\%$ ). However, the peak emission energy in this case is well below the BATSE range, since most of the emission originates at large radii, much larger than the radius of the photosphere  $R_\pm$ , the radius at which the wind becomes optically thin to Thomson scattering by  $e^\pm$  pairs [see the discussion preceding Eq. (5) in §3.2].

The dynamical efficiency in the case of a bimodal LF distribution can reach 50%, since the Lorentz factors of the colliding shells are very different. Contrary to the case of modulated ejection, the collisions at the photospheric radius  $R_\pm$  dominate wind emission, and a region of the parameter space exists, where model radiative efficiency and peak emission energy are consistent with observations,  $\epsilon_\gamma > 10\%$  and  $\epsilon_p \sim 100$  keV.

The case of a lognormal LF distribution can be considered as an intermediate case between the random and bimodal ones. In this case the maximal radiative efficiency expected is of the order 10-15%, much lower than the 80-90% value derived in Beloborodov (2000). This is due to the pair optical depth, which sets a lower limit of  $\Gamma_m \gtrsim 100$  for an optically thin wind (see §3.2 below), and to the constraint imposed on the maximum LF by finite source size,  $\Gamma_M < \eta_* \sim 10^{3.5}$ . These constraints limit the variance of the LF distribution, and hence the dynamical efficiency.

Considering shells of equal energy, rather than of equal mass, the main results do not change. Uniform LF distribution is still characterized by low efficiency and modulation leads to low peak emission energy. In the case of a bimodal distribution, the efficiency is lower for shells of equal energies than for shells of equal mass, due to an increase in wind optical depth. The LF of the merged shell, given by Eq.(3), is reduced in the equal energy case by a factor  $\sqrt{\Gamma_M/\Gamma_m}$  with respect to the equal mass case. Thus, the average wind LF is lower, implying smaller collision radii and higher opacity.

From the analysis of Fig. 1 we conclude that a bimodal distribution of shell LFs, that is, LF distribution with large variance, and equal shell mass are favored by observations. Note, that this conclusion is independent of the assumption of near equipartition, using which the above calculations were performed, since for electron and magnetic field energy fractions below equipartition the peak emission energy  $\epsilon_p$  would be lower than obtained above [see also §3.2, Fig. 4 and Eq. (9), below]. In what follows we study the bimodal LF case in more detail, in order to examine the dependence of observable characteristics on wind parameters.

### 3.2. Bimodal LF distribution

Figures 2 and 3 present the dependence on  $\Gamma_m$  and on  $t_v$  of peak emission energy,  $\epsilon_p$ , and radiative efficiency,  $\epsilon_\gamma$ , respectively, for  $\Gamma_M = 2500$ ,  $L_w = 10^{52} \text{ erg s}^{-1}$ ,  $R_0 = 10^6 \text{ cm}$  and equal shell masses. Results are presented in Fig. 2 for the two extreme assumptions on shell width evolution with radius,  $\Delta = R_0$  and  $\Delta = \max(R_0, R/\Gamma^2)$ . The efficiency contour plot, shown in Fig. 3, is

similar for both cases.

The dependence of  $\varepsilon_p$  on parameters can be understood considering the dependence of the dynamical efficiency and of the optical depth on  $\Gamma_m$  and  $t_v$ . For high values of  $\Gamma_m$  ( $> 300$ ), both reverse and forward shocks are optically thin. Decreasing  $\Gamma_m$  leads to a decrease in the initial radius of the collisions, increasing the efficiency up to 15% and the peak emission energy up to 0.1–1 MeV. At lower values of  $\Gamma_m$ , the efficiency decreases and steep breaks are observed in the  $\varepsilon_p$  contour plot. These breaks can be understood considering the difference between the FS and RS efficiencies, due to different comoving densities of the two colliding shells ( $E_f/E_r \sim \rho_{c,r}/\rho_{c,f}$ ). In the case of maximal shell expansion,  $\Delta = R/\Gamma^2$ , the ratio  $E_f/E_r \sim \Gamma_r/\Gamma_f$ , and the FS dominates the emission. Thus, the break in the  $\varepsilon_p$  contour plot (left panel of Fig. 2) corresponds to the region of  $\Gamma_m$  and  $t_v$  values where the FS, and consequently also the RS, become optically thick due to pair production ( $\Gamma_m = 50$  to  $\Gamma_m = 130$  for  $t_v$  varying between 1 s and  $10^{-4}$  s respectively). A small decrease in  $\Gamma_m$  results in collisions below the photosphere, leading to a steep decrease in peak emission energy, to a value corresponding to the second set of collisions, which occur at larger radii. These collisions dominate the emission and are characterized by a lower efficiency and a lower peak emission energy. In the case of a constant shell width  $\Delta = R_0$ , the ratio  $E_f/E_r \sim \Gamma_f/\Gamma_r$ , and the RS dominates the emission. Thus, there are two breaks in the peak energy contour plot (right panel of fig 2). The first corresponds to the values of  $\Gamma_m$  and  $t_v$  where the RS becomes optically thick due to pair production and the FS starts to dominate the emission. This break represents the shift of the peak energy from the RS value to the FS one. The other occurs in the parameter region where the FS becomes optically thick, and corresponds to the shift of the peak energy from the first to the second set of collisions.

The contour plot of the radiative efficiency in Fig. 3 shows that values of  $\epsilon_\gamma$  higher than 10% and peak emission energy between 0.1 and 1 MeV are reached at similar regions in the  $\Gamma_m - t_v$  plane, in accordance with the correlation between the peak emission energy and radiative efficiency shown in Fig. 1. High efficiency,  $> 10\%$ , is obtained only for large  $\Gamma_M$ ,  $\Gamma_M \approx \eta_* \approx 2 \times 10^3$ , i.e. for values close to the maximum allowed by the finite source size. For lower values of  $\Gamma_M$ , the dynamical efficiency decreases leading to lower  $\varepsilon_p$  and  $\epsilon_\gamma$ .

In Fig. 4 we present results of calculations similar to those presented in Fig. 2, for  $\epsilon_e$  and  $\epsilon_B$  values below equipartition. The results demonstare that the electron and magnetic field energy fractions can not be far below equipartition,  $\epsilon_e \gtrsim 10^{-1}$  and  $\epsilon_B \gtrsim 10^{-2}$  are required in order to obtain peak emission energies consistent with observations. These results are consistent with our analytic estimates, Eqs. (8) and (9) below.

The contour plot shown in Fig. 2 demonstrates that values of  $\varepsilon_p$  larger than  $\sim 1$  MeV can not be obtained. This result can be understood using the following arguments. For a collision of shells of thickness  $\Delta$  at radius  $R$ , we have

$$\varepsilon_p \approx \gamma_{min}^2 \frac{he}{2\pi m_e c} \sqrt{\frac{2\epsilon_B E_{in}}{R^2 \Delta}}. \quad (5)$$

The maximal value of  $\varepsilon_p$  is obtained for collisions at the smallest radius  $R$  for which the wind is optically thin. The radius of the Thomson photosphere due to the electrons present in the original fireball is given by

$$R_T \approx \sqrt{\frac{\sigma_T M}{4\pi m_p}} \approx 6 \times 10^{11} \text{ cm} L_{w,52}^{1/2} t_{v,-3}^{1/2} \Gamma_{M,3}^{-1/2}, \quad (6)$$

where  $M$  is the shell mass, and we have approximated  $M = L_w t_v / c^2 (\Gamma_m + \Gamma_M)$ .  $R_{\pm}$ , the Thomson photosphere radius due to  $e^{\pm}$  pairs resulting from pair production interaction of synchrotron photons, can be estimated by assuming that a significant fraction,  $\sim 1/2$ , of the radiative energy is converted to pairs, as typically is the case. The number density of  $e^{\pm}$  is given in this case by  $n_{\pm} \approx \epsilon_e E_{\text{in}} / (8\pi m_e c^2 R^2 \Gamma^2 \Delta)$  and

$$\begin{aligned} R_{\pm} &\approx \sqrt{\frac{3\sigma_T/16}{8\pi m_e c^2}} \sqrt{\frac{\epsilon_e E_{\text{in}}}{\Gamma}} \\ &\approx 10^{13} \text{ cm} \epsilon_e^{1/2} L_{w,52}^{1/2} t_{v,-3}^{1/2} (\Gamma_{M,3} \Gamma_{m,2})^{-1/4}. \end{aligned}$$

Comparing  $R_{\pm}$  and  $R_T$ , we conclude that the optical depth is typically dominated by the pairs.

For fixed  $t_v$  and  $\Gamma_M$ , the maximal peak energy is obtained for  $\Gamma_m = \Gamma_{m\pm}$  for which the collision radius  $R_i \approx \Gamma_m^2 c t_v$  equals the photospheric radius  $R_{\pm}$ . Solving for  $\Gamma_{m\pm}$ ,

$$\Gamma_{m\pm} \approx 5 \times 10^2 \epsilon_e^{2/9} \Gamma_{M,3}^{-1/9} t_{v,-3}^{-2/9} L_{w,52}^{2/9}, \quad (7)$$

and substituting in Eq. (5) we find

$$\varepsilon_p^{\max} \approx 2 \text{ MeV} \epsilon_B^{1/2} \epsilon_e^{4/3} \Gamma_{M,3}^{4/3} \Delta_6^{-1/2} t_{v,-3}^{1/6} L_{w,52}^{-1/6}, \quad (8)$$

where we have used  $\gamma_{\min} = \sqrt{(\Gamma_M / \Gamma_m)} \epsilon_e m_p / m_e \log(\gamma_{\max} / \gamma_{\min})$  with  $\gamma_{\max} = 100 \gamma_{\min}$ . The dependence of  $\varepsilon_p$  on wind luminosity is demonstrated in figures 5 and 6. Under the assumption of fixed shell width,  $\Delta = R_0$ ,  $\varepsilon_p^{\max}$  is weakly dependent on  $L$ , as indicated by Eq. (8). If the maximum Lorenz factor scales as  $\Gamma_M \approx \eta_* \propto L^{1/4}$ , rather than being independent of  $L$ , the slow decrease with  $L$  of  $\varepsilon_p^{\max}$  at fixed  $t_v$ ,  $\varepsilon_p^{\max} \propto L^{-1/6}$ , is replaced by a slow increase with  $L$

$$\varepsilon_p^{\max} \approx 4 \text{ MeV} \epsilon_B^{1/2} \epsilon_e^{4/3} \Delta_6^{-5/6} t_{v,-3}^{1/6} L_{w,52}^{1/6}. \quad (9)$$

The dependence on luminosity becomes stronger under the assumption of maximal expansion. Substituting  $\Delta = R / \Gamma^2$  in Eq. (8), we find  $\varepsilon_p^{\max} \propto L^{-5/18}$ . The stronger dependence is also apparent in figures 5 and 6. However, allowing for a scaling  $\Gamma_M \approx \eta_* \propto L^{1/4}$ , the peak emission energy dependence on  $L$  becomes  $\varepsilon_p^{\max} \propto L^{7/36}$ , similar to the dependence shown in Eq. (9).

#### 4. Conclusions

We have analyzed a model of GRBs, in which a compact source of linear scale  $R_0$  produces a wind characterized by an average luminosity  $L_w$  and mass loss rate  $\dot{M} = L_w / \eta c^2$ . At small

radius, the wind bulk Lorentz factor,  $\Gamma$ , grows linearly with radius, until most of the wind energy is converted to kinetic energy and  $\Gamma$  saturates at  $\Gamma \sim \eta$ . Variability of the source results in fluctuations in the wind saturation Lorentz factor  $\Gamma$ , leading to internal shocks in the expanding wind. These shocks reconvert a fraction of the kinetic energy back to internal energy, which is assumed to be radiated as  $\gamma$ -rays by synchrotron (and inverse-Compton) emission of shock-accelerated electrons. Since the wind duration,  $t_w \sim 10$  s, is much larger than the dynamical time of the source,  $t_d \sim R_0/c$ , variability of the wind on a wide range of time scales,  $t_d < t_v < t_w$ , is possible. For simplicity, we have assumed that in addition to  $t_d$ , which determines the initial shell thickness  $\Delta = ct_d \sim R_0$ , and  $t_w$ , the wind is characterized by a single time scale  $t_v > t_d$ , which determines the shell ejection rate  $t_v^{-1}$ . We have addressed the questions of whether, and under what conditions, high radiative efficiency consistent with observations can be obtained, and whether the observed clustering of peak emission energies can be naturally explained by the model.

We have shown that a significant fraction,  $\sim 15\%$ , of the fireball energy can be converted to radiation. As pointed out at the end of §2, our simplified treatment of post-collision shell evolution, assuming complete merger of shells, leads to an overestimate of the reduction of the variance of colliding shells' Lorenz factors with wind evolution. A more detailed calculation of the merger process will lead to an enhancement of the radiative efficiency by a factor of order unity. The exact value of the enhancement factor will depend, however, on the unknown internal shell structure. Adopting simplifying assumptions regarding the shell structure and post-collision evolution, Kobayashi & Sari (2001) have recently pointed out that including post-collision evolution effects may lead to radiative efficiency exceeding  $\epsilon_e$  (note, that this may be the case also when post-collision evolution is neglected). Although this effect may relax somewhat the constraint imposed on  $\epsilon_e$  by the requirement of high efficiency, we have shown here (see following paragraph), that  $\epsilon_e$  is constrained to be of order unity by the observed  $\gamma$ -ray spectra.

In order to obtain high radiative efficiency and peak emission energy  $\sim 1$  MeV, the minimum radius  $R_i$  at which internal collisions in the expanding wind occur is required to be similar to  $R_{\pm}$ , the radius where the Thomson optical depth due to  $e^{\pm}$  pairs produced by shock synchrotron emission equals unity [see Eq. (7)], and a large variance (compared to the mean) of the colliding shells' Lorenz factor (LF) distribution is required. In addition, the electron and magnetic field energy fractions should be close to equipartition, with  $\epsilon_e \gtrsim 0.1$  and  $\epsilon_B \gtrsim 0.01$ , in order for model predictions to be consistent with the observed peak emission energy distribution [see Fig. 4 and Eq.(9)]. The constraint  $R_i \sim R_{\pm}$  is equivalent to a constraint on the minimum LF,  $\Gamma_m$ , of expanding shells,  $\Gamma_m \sim \Gamma_{m\pm} \approx 10^{2.5}(L_{w,52}/t_{v,-3})^{2/9}$ , where  $L_w = 10^{52}L_{w,52}\text{erg s}^{-1}$  and  $t_v = 10^{-3}t_{v,-3}$  s [see Eq. (7)]. Large variance in the LF distribution of colliding shells than requires a non-uniform LF distribution (e.g. truncated log-normal or bimodal distributions, see Fig. 1) with  $\Gamma_M$ , the maximum LF of wind shells, close to the upper limit set by the shell acceleration process,  $\Gamma < \eta_* \approx (\sigma_T L_w / 4\pi m_p c^3 R_0)^{1/4} = 2 \times 10^3 (L_{w,52}/R_{0,6})^{1/4}$ , where  $R_0 = 10^6 R_{0,6}$  cm.

Our results do not agree with the very high,  $\sim 80\%$ , radiative efficiency values, obtained in

the calculations of Beloborodov (2000) and Kobayashi & Sari (2001) by assuming wind Lorentz factor distributions extending from  $\Gamma_m \sim 10$  to  $\Gamma_M \gtrsim 10^4$ . In our opinion the minimum wind Lorentz factor must be significantly higher than 10 (as otherwise the wind becomes optically thick) while the maximum Lorentz factor can not significantly exceed  $10^3$  (due to the acceleration process limitations).

We have shown that there is an upper limit to the observed energy of photons,  $\varepsilon_p$ , at which the  $\gamma$ -ray flux peaks,  $\varepsilon_p \lesssim \varepsilon_p^{\max} \approx 0.5R_{0,7}^{-5/6}$  MeV (where  $R_0 = 10^7 R_{0,7}$  cm), with very weak dependence on  $L_w$  and on  $t_v$  [see discussion preceding Eq. (9), and figures 2, 5 and 6]. Thus, the source dynamical time  $t_d \sim R_0/c$  must satisfy  $t_d \lesssim 1$  ms in order to allow  $\varepsilon_p \sim 1$  MeV.  $\varepsilon_p \approx \varepsilon_p^{\max}$  is obtained for  $\Gamma_m \approx \Gamma_{m\pm}$ , for which the radiative efficiency is largest, and  $\varepsilon_p$  values in the range of 0.1 MeV to 1 MeV are obtained for wind parameters for which the radiative efficiency is high,  $\gtrsim 10\%$  (see figure 3).

High radiative efficiency and peak emission energy consistent with observations are therefore obtained for  $\Gamma_m \sim \Gamma_{m\pm}$ . This does not necessarily imply that fine tuning of this model parameter is required. For  $\Gamma_m < \Gamma_{m\pm}$ , most efficient collisions occur at radii where the optical depth is high, leading to low efficiency, and hence low luminosity, bursts with peak emission energy  $\sim 1$  keV (see figures 2 and 3), which would not have been detected by BATSE. For  $\Gamma_m$  significantly higher than  $\Gamma_{m\pm}$ , LF variance is small, leading to low efficiency, low luminosity bursts with peak emission energy  $\sim 10$  keV, which may have been difficult to detect with BATSE. Natural consequences of the model considered here are therefore absence of bursts with peak emission energy significantly exceeding  $\sim 1$  MeV, and existence of low luminosity bursts with low,  $\sim 1$  keV to  $\sim 10$  keV, peak emission energy. The frequency of such bursts depends on the distribution of  $\Gamma_m$  in different winds.

It should be pointed out in this context that while the deficit, among bursts detected by BATSE, of bursts with peak emission energy below  $\sim 50$  keV clearly reflects a real deficit of such bursts, the deficit in detected bursts with peak emission energy  $> 0.5$  MeV may be partly due to a selection effect (e.g. Llyod & Petrosian 1999). BATSE data are consistent with equal number of bursts per logarithmic peak energy interval beyond  $\varepsilon_p \sim 0.5$  MeV (with luminosity comparable to that of lower peak energy bursts). Our model prediction, that bursts with  $\varepsilon_p \gg 1$  MeV should be absent, should therefore be tested with future GRB detectors, which are able to better constrain the high energy end of the  $\varepsilon_p$  distribution.

A note should be made here regarding the low energy spectral slope. The upper limit  $\eta_*$  on  $\Gamma_M$  is a consequence of the fact that for  $\eta > \eta_*$  shell acceleration saturates at  $\Gamma \sim \eta_* < \eta$ , as the wind becomes optically thin to Thomson scattering, and the internal energy left in the shell escapes as thermal radiation rather than being converted to kinetic energy. The requirement  $\Gamma \sim \eta_*$  therefore implies that a significant fraction of the wind energy may escape as thermal radiation, leading to low energy spectral slopes steeper than those expected for pure synchrotron emission. This may account, at list partially, for observed steep low energy spectra.

Finally we note that the lower limit imposed on  $\Gamma_m$ ,  $\Gamma_m \gtrsim \Gamma_{\pm}$ , is not derived from the requirement that the pair production optical depth for high energy,  $> 100$  MeV, photons be smaller than unity. While this requirement leads to a similar constraint,  $\Gamma_m \gtrsim 10^2$ , high energy photons have been detected in a small number of cases only. The constraint  $\Gamma_m > \Gamma_{m\pm}$  is imposed in the present analysis by the requirement that the wind Thomson optical depth due to  $e^{\pm}$  pairs produced by synchrotron photons be smaller than unity at the internal shocks stage.

The research of DG and MS is supported by COFIN-99-02-02. EW is partially supported by BSF Grant 9800343, AEC Grant 38/99 and MINERVA Grant. We thank Marco Salvati for useful comments on the manuscript. D.G. and M.S. thank the Weizmann Institute of Science, where part of this research was carried out, for the hospitality and for the pleasant working atmosphere.

## REFERENCES

Band, D. et al. 1993, *ApJ*, **413**, 281

Beloborodov, A.M. 2000, *astro-ph/0004360*

Brainerd, J.J et al. 1999, Abstract of the 19th Texas Symposium on Relativistic Astrophysics and Cosmology, Paris, 1998.

Costa, E. et al. 1997, *Nature*, **387**, 783

Daigne, F. & Mochkovitch, R., 1998, *MNRAS*, **296**, 275

Derishev, E.V., Kocharovskiy, V.V. & Kocharovskiy, VL.V. *astro-ph/0006239*

Frail, D. A., Waxman, E., & Kulkarni, S. R. 1999, *Ap. J.* **537**, 191.

Frail, D. et al. 1997, *Nature*, **389**, 261

Freedman, D. & Waxman, E., *ApJ* in press (*astro-ph/9912214*)

Frontera, F. et al. 2000, *ApJS*, **127**, 59

Lazzati, D. et al. 2000, *ApJ*, **529**, L529

Kats, J.I. 1994, *ApJ*, **432**, L107

Kobayashi, S., Piran, T. & Sari, R. 1997, *ApJ* 490, 92.

Kobayashi, S. & Sari, R. 2001, submitted to *ApJ* (*astro-ph/0101006*).

Kumar, P. 1999, *ApJ*, **523**, L113

Kumar, P. & Piran, T. 2000, *ApJ*, **535**, 152

Llyod, N. M. & Petrosian, V. 1999, ApJ 511, 550.

Mészáros, P. 1995, in Proc. 17th Texas Conf. Relativistic Astrophysics, Annals Ny. Acad. Sci. No. 759 (NY Acad. Sci., NY)

Mészáros, P., & Rees, M.J. 1997, ApJ, **476**, 232

Mészáros, P., & Rees, M.J. 2000, ApJ, **530**, 292

Paczyński, B., & Rhoads, J., 1993, ApJ, **418**, L5

Panaitescu & Mészáros, astro-ph/9810258.

Panaitescu, A., Spada, M. & Mészáros, P. 1999, **526**, 707

Piran, T. 1996, in Unsolved Problems In Astrophysics (eds. J. N. Bahcall and J. P. Ostriker), 343-377 (Princeton, 1996)

Preece, R. D. *et al.* 1998, ApJ, **506**, L23

Sari, R. & Piran, T. 1997, ApJ, **485**, 270

Spada, M., Panaitescu, A., & Mészáros, P. 2000, ApJ, **537**, 824

van Paradijs, J. *et al.* 1997, Nature, **386**, 686

Vietri, M. 1997, ApJ, **478**, L9

Waxman, E. 1997, ApJ, **485**, L5

Wijers, R., Rees, M.J., Mészáros, P. 1997, MNRAS, 288, L51

Woods, E. & Loeb, A., Ap. J. **453**, 583 (1995).

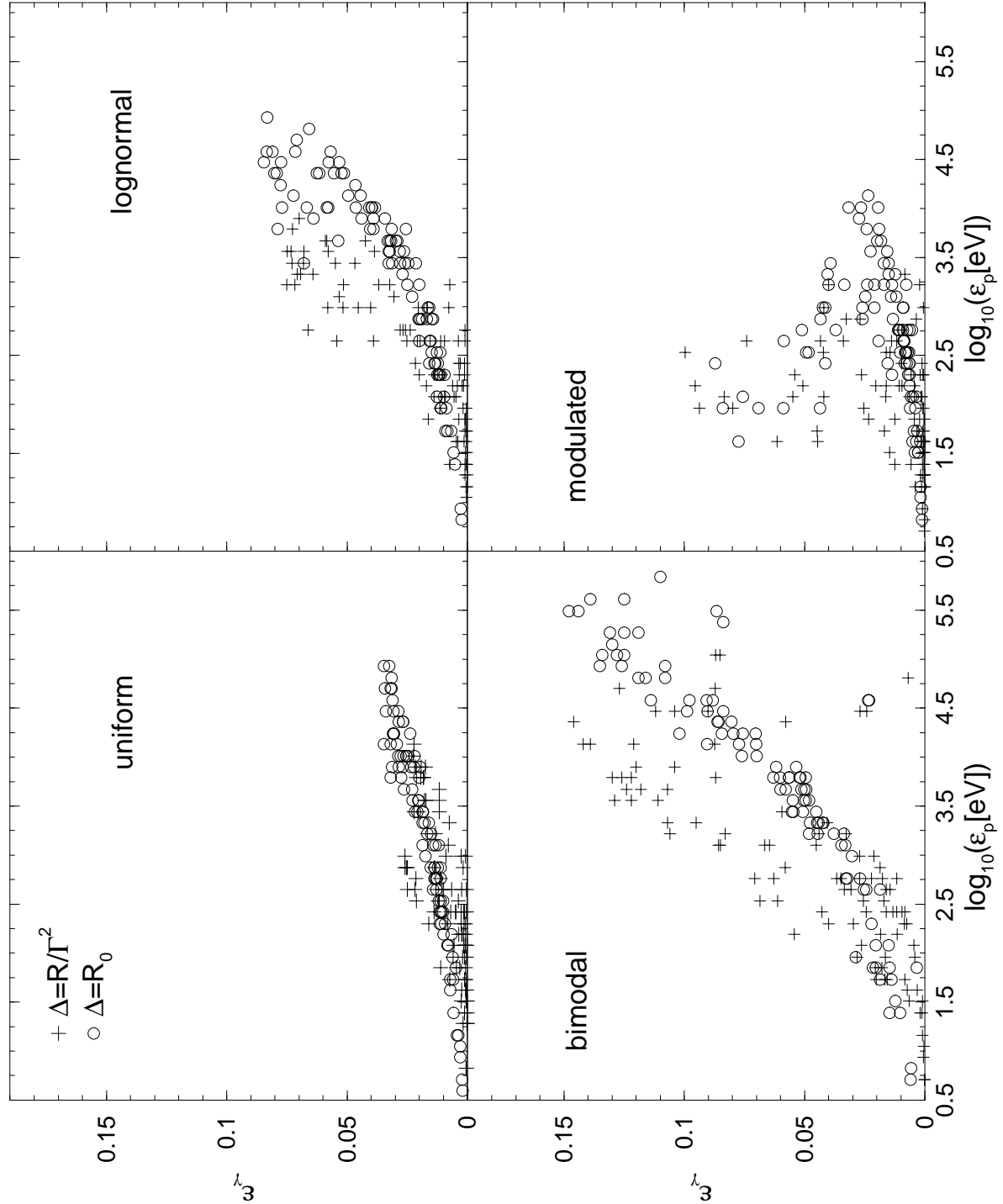


Fig. 1.— Radiative efficiency versus peak emission energy for various Lorenz factor distributions. Different points within each panel correspond to different choices of  $\Gamma_m$ ,  $\Gamma_M$  and  $t_v$ . Results are shown for  $10 < \Gamma_m < \Gamma_M < 2500$  and  $10^{-4} \text{ s} < t_v < 1 \text{ s}$ , for two extreme assumptions on shell width expansion, maximal expansion  $\Delta = \max(R_0, R/\Gamma^2)$  and constant width  $\Delta = R_0$ . We have assumed equal mass shells,  $R_0 = 10^6 \text{ cm}$ ,  $L_w = 10^{51} \text{ erg s}^{-1}$  and source redshift  $z = 1$  for all calculations.

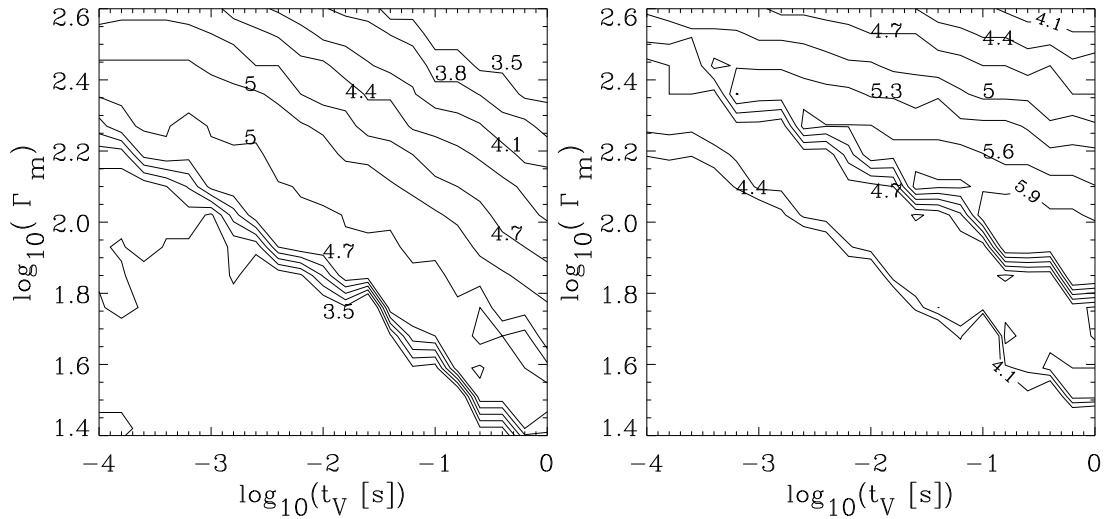


Fig. 2.— Contour plots of the peak emission energy,  $\log_{10}(\varepsilon_p[\text{eV}])$ , as a function of  $t_v$  and the minimum Lorentz factor  $\Gamma_m$  of the ejected shells. The value of  $\Gamma_M$  is 2500 and  $L_w = 10^{52} \text{ erg s}^{-1}$ , the LF distribution is bimodal and the shells have equal masses. The left panel refers to the case of expanding shell  $\Delta = \max(R_0, R/\Gamma^2)$  and the right panel to the case of time independent shell thickness  $\Delta = R_0$ .

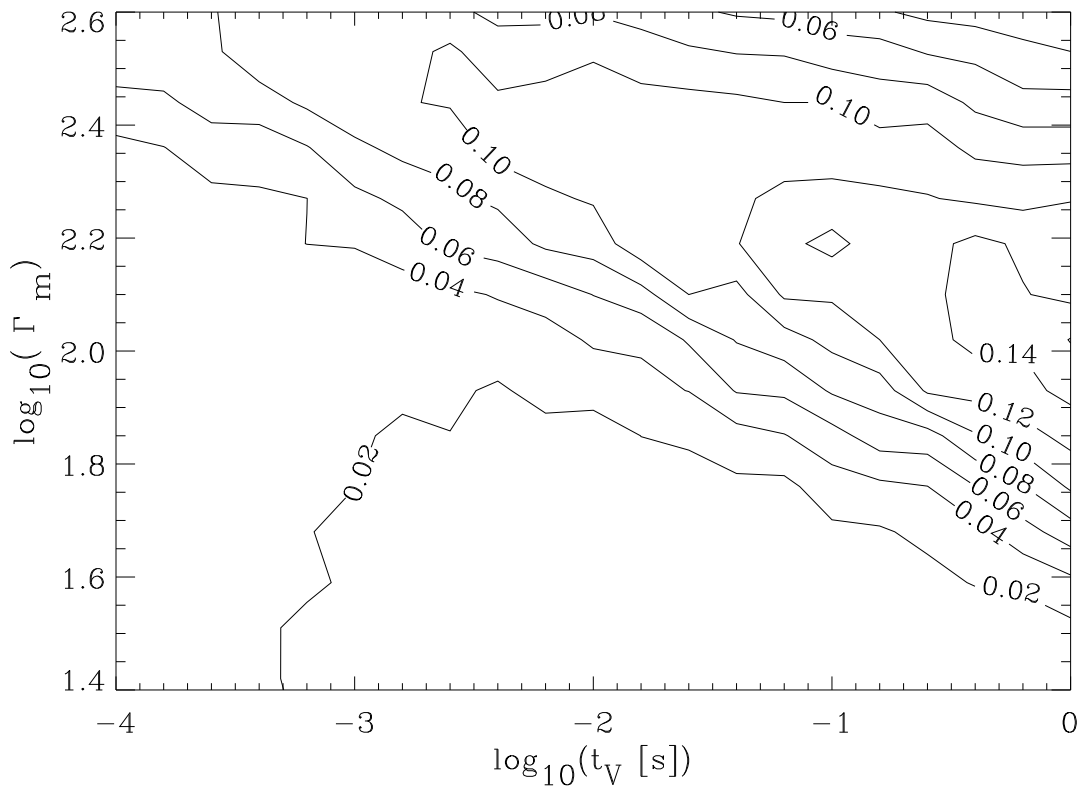


Fig. 3.— Contour plot of the radiative efficiency for the case described in Fig. 2. The radiative efficiency is similar for both  $\Delta = \max(R_0, R/\Gamma^2)$  and  $\Delta = R_0$  cases.

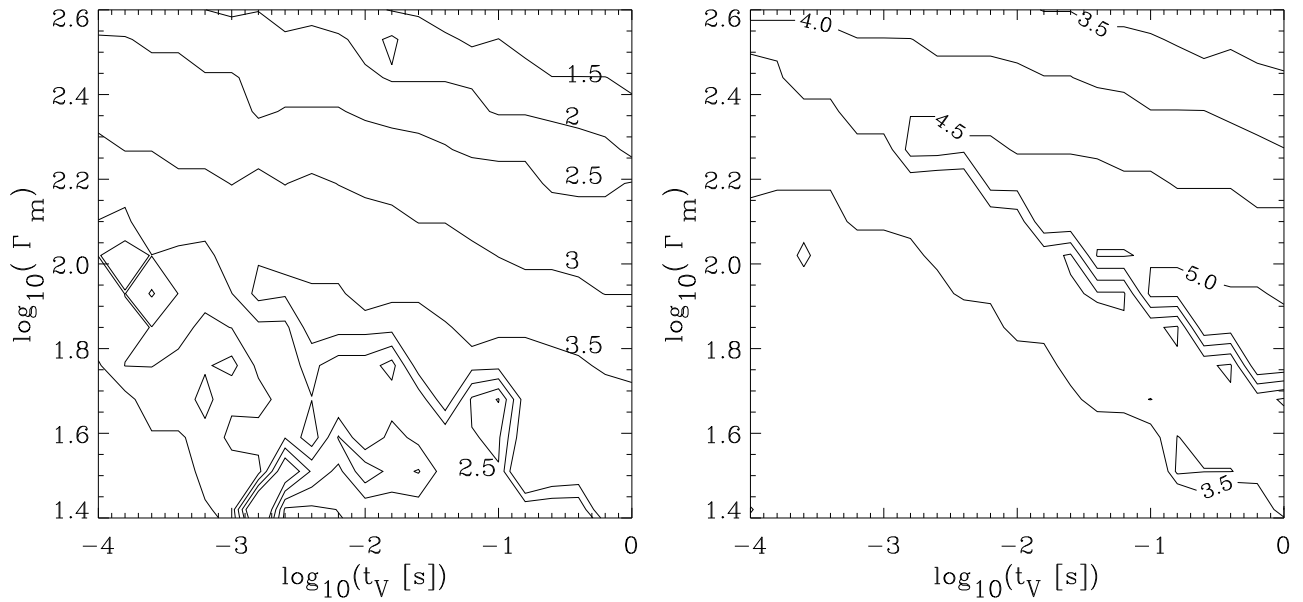


Fig. 4.— Same as right panel of Fig. 2 (constant pre-shock shell width), for electron and magnetic field energy fractions below equipartition. Left panel:  $\epsilon_e = 0.01$ ,  $\epsilon_B = 0.1$ ; Right panel:  $\epsilon_e = 0.45$ ,  $\epsilon_B = 0.001$ .

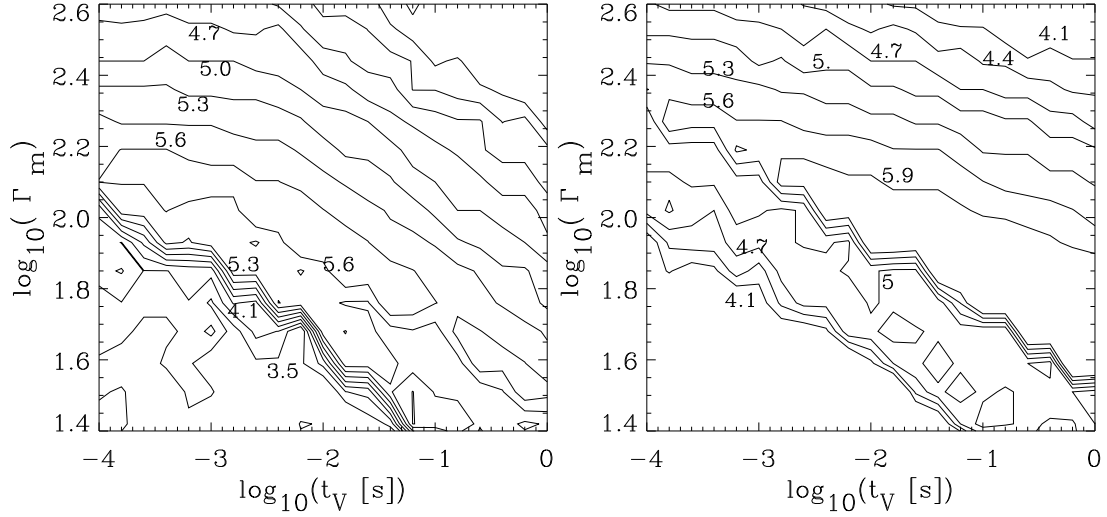


Fig. 5.— Same as Fig. 2, for different luminosity,  $L_w = 10^{51} \text{ erg s}^{-1}$ .

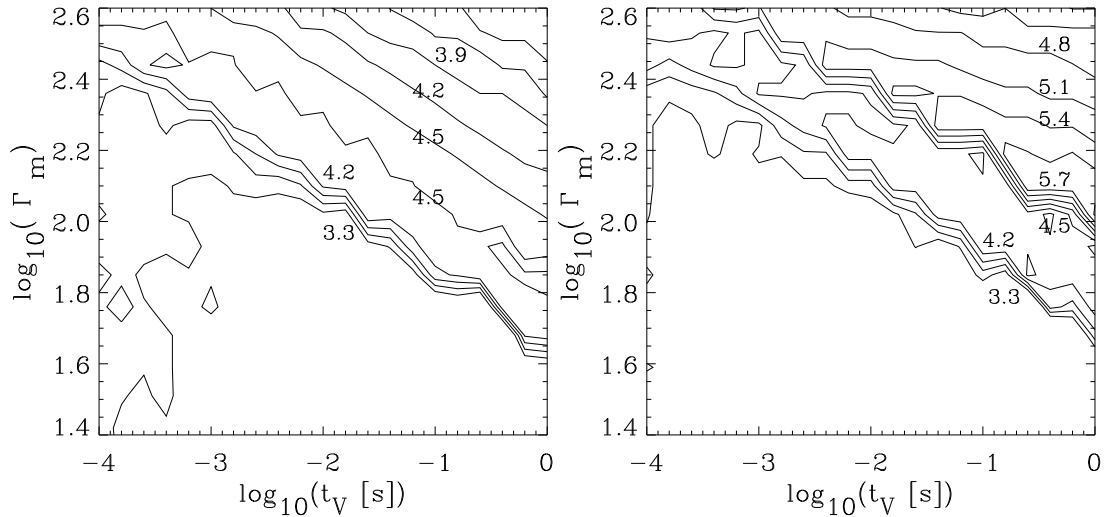


Fig. 6.— Same as Fig. 2, for  $L_w = 10^{53} \text{ erg s}^{-1}$ .